Motion Planning of Extreme Locomotion Maneuvers Using Multi-Contact Dynamics and Numerical Integration

Luis Sentis and Mike Slovich (lsentis@austin.utexas.edu, michael.slovich@gmail.com)

***Abstract*—Although the problem of maneuvering in extreme terrains has critical weight on the advancement of legged robots and medical assistive devices, little progress has been made on exploring practical solutions to operate in these environments. Here, we report that multi-contact models and perturbation theory, a set of approximation schemes that has roots in celestial mechanics and non-linear dynamical systems, can be adapted to solve non closed-form integrable state-space trajectories of a robot's center of mass, given its arbitrary contact state and center of mass (CoM) path. In this paper we explore a case study of an extreme maneuver involving gap leaping given a support point against a wall board to ascend steps on a ladder. To tackle this problem, we first leverage our previous work on multi-contact dynamics to derive reaction force behavior from inertial movement and internal tension behavior. We then study the nonlinear dynamics of single contact phases along arbitrary paths and leverage perturbation theory to derive state space equations of center of mass behavior.**

Using this theoretical framework, we consider synthesizing extreme maneuvers in the terrain by means of a motion planner. We derive kinematic trajectories that fulfill dynamic constraints, such as the center of mass' angle of attack. We then use numerical integration to solve the natural dynamics of the robot along the planned path. We leverage our derivations on multi-contact dynamics to search the space of feasible movements and internal tension behaviors during multi-contact. Finally, we propose a new strategy to determine step transitions during jumping and landing maneuvers. Our main contributions are on, (1) developing a methodology to use the multi-contact/grasp matrix and numerical integration to derive state space trajectories of extreme maneuvers, and (2) developing a motion planner that can determine contact transitions to negotiate the terrain.

I. Motivation

Free-running is the ability to perform extreme maneuvers in urban or back terrain by using fast contact interactions with surrounding structures. Humans and animals are capable of maneuvering with relative ease in these environments but little is known on the nature of these type of skills, in part due to the limited availability of modeling and planning methods. As such, our hypothesis, is that by modeling extreme movements we will create new opportunities in the areas of path planning and control of humanoid robots and assistive devices. In turn, this research has wider potential to enable the development of practical outdoor assistive devices as well as on health related fields.

In this paper we take on a case of an extreme maneuver inspired by the sport of free-running and use it to produce models of movement and synthetic plans that can handle similar terrains. The importance of this study lies on the lack of substantial scientific material on the subject and on the prospect to apply legged systems in urban and back terrain. Moreover, this study could enable one day to mechanically outperform human capabilities because of its focus on extreme skills.

Some of the main challenges for successfully studying extreme maneuvers are the absence of mathematical tools to characterize these type of movements, the lack of understanding of extreme physical interactions, and the inadequacy of motion planners to artificially synthesize these motions. In particular, it is known that extreme maneuvers can be expressed in terms of nonlinear dynamical models but, unfortunately, do not have a closed solution to work with, posing a challenge on extracting the behaviors. Moreover, extreme maneuvers are not only governed by natural inverted pendulum dynamics but also by internal forces during multi-contact phases. Last but not least, motion planners that can synthesize extreme maneuvers do not exist due to the difficulty of finding contact transitions.

Our contributions are a direct response to these challenges. First, we incorporate multi-contact models to the generation of center of mass behavior and we propose search-based techniques to extract maneuvering patterns. We then use perturbation theory to obtain phase curves of center of mass behavior associated with the contact states. Finally, we propose a motion planner consisting on deriving phase curves for single and multi-contact phases and finding the points of intersection between phases to determine contact transitions.

II. Background

In dynamic walking we can classify techniques in various categories: (1) trajectory-based techniques, (2) passive dynamic walking and optimal control, (3) prediction of contact, and (4) hybrids of the previous three.

Trajectory-based techniques are techniques that track a time-based joint or task space trajectory according to some locomotion model such as the Zero Moment Point (ZMP). The state of the art of these methods includes generalized multi-contact locomotion behaviors, developed in [1] and more recently, a time delay extension to the ZMP method for locomotion in moderately uneven terrain, developed by [2].

Prediction of contact placement are techniques that use dynamics to estimate suitable contact transitions to produce locomotion or regain balance. In [3], simple dynamic models are used to predict the placement of next contacts to achieve desire gait patterns. Finding feasible CoM static placements given frictional constraints was tackled in [4], [5]. In [6], stable locomotion, in the wide sense of not falling down, is studied by providing velocity based stability margins. This work is used to regain stability when the robot's is pushed out, and lead to the concept of Capture Point.

Passive dynamic walking and optimal control were pioneered by McGeer [7] through the field of passive dynamic walking. In [8] the authors study orbital stability, and the effect of feedback control to achieve asymptotic stability. Optimization of open-loop stability is investigated in [9]. In [10], [11], [12], the authors analyze the energetic cost of bipedal walking and running as well as the role of leg sequencing. In [13], the authors developed a dynamic walker using artificial muscles and principles of stability of passive walkers. In [14], a methodology for the analysis of state-space behavior and feedback control are presented for various physical robots. Step recovery in response to perturbations is studied in [15] supported by a linear bipedal model in combination with an orbital energy controller. In [16], the selection of gait patterns based on studying the interplay between robustness against perturbations and leg compliance is investigated.

Hybrid methods include [17], where the stability of passive walkers is studied and a controller obeying the rule, "in order to prevent falling backward the next step, the swing leg shouldn't be too far in front", in the words of the author, is suggested. Stochastic models of stability and its application for walking on moderately rough unmodeled terrain are studied in [18]. The design of non-periodic locomotion for uneven terrain is investigated in [19], [20]. In [21], the authors explore the design of passivity-based controllers to achieve walking on different ground slopes. Optimization-based techniques for locomotion in rough terrains are presented in [22]. Locomotion in very rough terrain is presented in [23], where the authors exploit optimization and static models as a means to plan locomotion. More recently, the authors of [24] have proposed a very

efficient planner that can generate a discrete sequence of multi-contact stances using static criteria. Also very recently, we made various theoretical contributions [25], [26] to enable walking at fast speeds in very rough variable terrain.

III. Mathematical Derivations

A. Dynamic behavior from multiple contacts

Dynamic equilibrium of mechanical systems states that the sum of external and reaction forces and moments on a moving system equals the net inertial and gravitational forces and moments acting on it. In our paper [27] a multi-contact/grasp matrix describing the complex interactions between contact forces and center of mass behavior was developed based on the principle of dynamic equilibrium. Based on this study, we proposed a virtual linkage model for humanoid robots to analyze the inter-dependencies between whole-body contacts and center of mass behavior.

In particular, we consider the multi-contact scenario shown in Figure 3 where a human performs an extreme maneuver involving fast swings of his body back and forth using the two feet contacts placed against uneven surfaces. For simplicity, we model the feet as point contacts. In such case, the multi-contact/grasp matrix can be derived from the virtual linkage model [27] as

$$\begin{pmatrix} f_{\text{com}} + Mg \\ m_{\text{com}} \\ f_t \end{pmatrix} = C_{7\times 6} \begin{pmatrix} f_{r(RF)} \\ f_{r(LF)} \end{pmatrix}, \tag{1}$$

where $f_{r(RF)}$ and $f_{r(LF)}$ represent the three dimensional reaction forces on the right and left feet, respectively, $f_{\text{com}} \triangleq M\, a_{\text{com}}$ represents inertial forces caused by center of mass accelerations, a_{com} is the three dimensional vector of center of mass linear accelerations, M is the total mass of the human, $g \triangleq (0,\ 0,\ 9.81)$ is the vector of gravitational accelerations pointing upward to be consistent with reaction forces, m_{com} is the three dimensional vector of inertial moments at the center of mass, and f_t is the one dimensional vector of internal tension forces between the feet.

The multi-contact/grasp matrix $C_{7\times 6}$, derived in the Appendix, is non-square and therefore non-invertible, prompting us to further study its structure. We further consider the decomposition of the multi-contact/grasp matrix given in Equation (35) focusing on the inertial components. An empirical study of the submatrix $W_{\text{com}\,6\times 6}$ (see Equations (32) and (35)) by means of the motion captured sequence of Figure 3, reveals that it has rank 5 instead of 6. Such condition is analogous to the dependencies between bipedal center of pressure points and center of mass accelerations that we analyzed in detail in [27]. One way to get around with this deficiency is to remove one raw from $W_{\text{com}\,6\times 6}$, for instance the raw corresponding to the linear forces in the lateral y direction. This can be achieved by considering the selection matrix described in Equation (36), which leads to the full rank expression

$$C_{6\times 6} \triangleq S_{\text{VL}}\, C_{7\times 6}. \tag{2}$$

Given the above dimensional reduction, we can now solve reaction forces for a given center of mass inertial and internal tension behavior, as

$$\begin{pmatrix} f_{r(RF)} \\ f_{r(LF)} \end{pmatrix} = C_{6\times 6}^{-1}\, S_{\text{VL}} \begin{pmatrix} f_{\text{com}} + Mg \\ m_{\text{com}} \\ f_t \end{pmatrix} \tag{3}$$

If we consider the block decomposition,

$$C_{6\times 6}^{-1}\, S_{\text{VL}} = \left(C_{f\,6\times 2} \mid C_{m\,6\times 3} \mid C_{t\,6\times 1} \right), \tag{4}$$

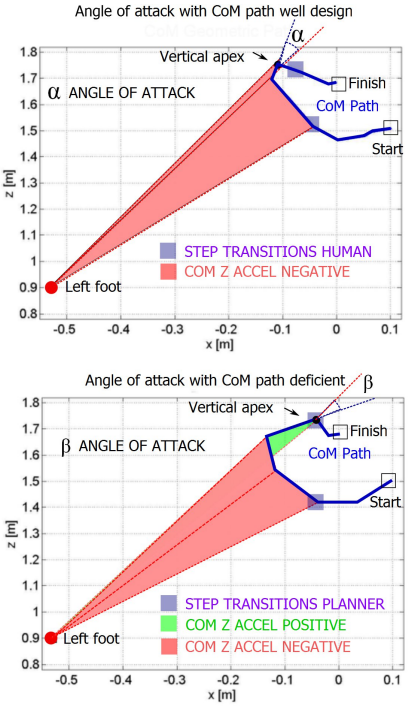

Fig. 1. **Angle of attack from single contact phase:** In these graphs we show the angle of attack for two different center of mass geometric paths. Only the one on the top is feasible since it is positive, i.e. $\alpha > 0$, resulting in a deceleration before reaching the vertical apex. On the other hand, the bottom graph has an angle of attack $\beta < 0$.

we can express the reaction forces in the more intuitive form

$$\begin{pmatrix} f_{r(RF)} \\ f_{r(LF)} \end{pmatrix} = C_f\, S_{xz} \left(f_{\text{com}} + Mg \right) + C_m\, m_{\text{com}} + C_t\, f_t \tag{5}$$

where

$$S_{xz} \triangleq \begin{pmatrix} 1 & 0 & 0 \\ 0 & 0 & 1 \end{pmatrix}, \tag{6}$$

is a subcomponent of S_{VL} that removes the y direction. Equation (5) will serve as our model to both analyze and also synthesize extreme multi-contact maneuvers.

B. Dynamic behavior from a single contact

Once more, we use the principle of dynamic equilibrium, this time around applied to a single contact. In particular, we consider the single contact scenario corresponding to the flight phase of Figure 4. In such case, the balance of dynamic moments can be formulated as

$$p_{\text{cop}_k} \times f_{r_k} = p_{\text{com}} \times \left(f_{\text{com}} + M\, g \right) + m_{\text{com}}, \tag{7}$$

where, k is the limb in contact with the wall board, p_{cop_k} is the limb's Center of Pressure (CoP) point, f_{r_k} is the 3-dimensional vector of reaction forces and f_{com} and m_{com} are 3-dimensional vectors of center of mass inertial forces and moments respectively. The above equation is vectorial and represents three orthogonal moments. Once more we have considered point contact for simplicity and therefore there are no reaction moments that need to be taken into account. Solving this equation for the CoP in the Sagittal direction (see [25]), leads to the solution

$$p_{\text{cop}_k[x]} = p_{\text{com}[x]} - \frac{f_{r[kx]}}{f_{r[kz]}} \left(p_{\text{com}[z]} - p_{\text{cop}_k[z]} \right) - \frac{m_{\text{com}[y]}}{f_{r[kz]}}. \tag{8}$$

Using the equalities $f_{r_{[kx]}} = M a_{\text{com}[x]}$, and $f_{r_{[kz]}} = M(a_{\text{com}[z]}+g)$ we can rewrite the above equation as

$$a_{\text{com}[x]} = \frac{\Big(p_{\text{com}[x]} - p_{\text{cop}_k[x]}\Big)\Big(a_{\text{com}[z]} + g\Big)}{p_{\text{com}[z]} - p_{\text{cop}_k[z]}} \tag{9}$$

Here, we have assumed a point mass model of the human or robot, with all of its weight located at its center of mass. As such, there are no inertial moments generated about the center of mass, i.e. $m_{\text{com}} = 0$. Simplifying moments represents a limitation that we are aware of and therefore we plan to consider more comprehensive models in the future. Also, note that a similar equation could be derived for accelerations in the lateral direction, but for the sake of simplicity we do not consider it in this study, thus restricting our initial results to Sagittal movements.

C. Geometric path planning

Because in Equation (9) there are two variables that need to be solved, i.e. the accelerations of the center of mass on the Sagittal and vertical directions, we choose to first seed geometric dependencies based on an initial guess. This is equivalent to choosing a geometric path of the center of mass a priori. There are many options to determine these dependencies, ranging from ensuring kinematic constraints, generating biomimetic patterns, or minimizing power. Let us consider the option of ensuring kinematic constraints only.

One simple dependency is to draw a piecewise linear geometric path of the humanoid's CoM behavior that fulfills robot kinematic constraints. Let us consider a given CoM geometric path determined by a kinematic planner and for the length of a given maneuver. Because the geometric trajectory is piecewise linear, it can be specified through equations of multiple intersecting lines, i.e.

$$p_{\text{com}[z]} = \begin{cases} a_1\, p_{\text{com}[x]} + b_1, & p_{\text{com}} \in \mathbb{P}_1 \\ a_2\, p_{\text{com}[x]} + b_2, & p_{\text{com}} \in \mathbb{P}_2 \\ \quad\vdots & \\ a_N\, p_{\text{com}[x]} + b_N, & p_{\text{com}} \in \mathbb{P}_N \end{cases} \tag{10}$$

where, $\mathbb{P}_j$ represents the path of the CoM over line segment j. Moreover, the acceleration profile can be extracted by differentiating twice the above piecewise equation, i.e.

$$\text{if } p_{\text{com}[z]} = a_i\, p_{\text{com}[x]} + b_i, \text{ then } a_{\text{com}[z]} = a_i\, a_{\text{com}[x]}. \tag{11}$$

Plugging the above acceleration in Equation (9) we get

$$a_{\text{com}[x]} = \frac{\Big(p_{\text{com}[x]} - p_{\text{cop}_k[x]}\Big)\Big(a_i\, a_{\text{com}[x]} + g\Big)}{a_i\, p_{\text{com}[x]} + b_i - p_{\text{cop}_k[z]}}, \tag{12}$$

and since $a_{\text{com}[x]}$ appears both on the left and right hand sides, we can rewrite the equation as

$$a_{\text{com}[x]} = \frac{\Big(p_{\text{com}[x]} - p_{\text{cop}_k[x]}\Big)\cdot g}{\Big(a_i\, p_{\text{cop}_k[x]} + b_i - p_{\text{cop}_k[z]}\Big)}. \tag{13}$$

Notice that the denominator and the second term in the numerator above are constants, so the above equation is of the form $\ddot{x} = \beta\,(x - \alpha)$, which is linear and as such has a closed-form solution.

However, in a more general case, kinematic paths are not based on piecewise linear functions, but instead depend on more sophisticated base functions. For instance, in legged locomotion an efficient gait can be produced by following circular arcs, i.e. $p_{\text{com}[z]} = \big(r^2 - p^2_{\text{com}[x]}\big)^{0.5}$. In that case path accelerations for a given step can be expressed by differentiating the arc, i.e.

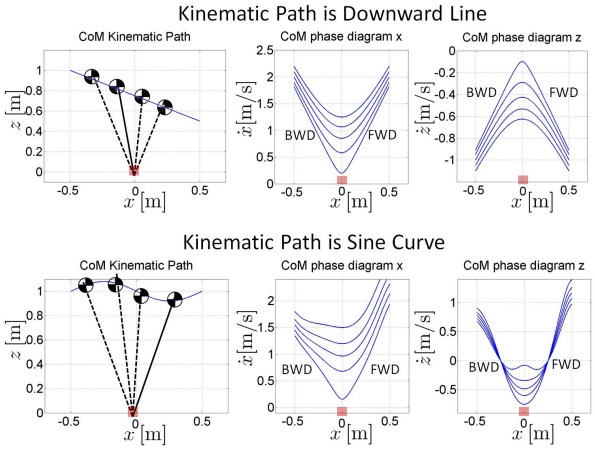

Fig. 2. **Phase diagrams of CoM behavior using perturbation theory:** These phase diagrams correspond to Matlab simulations of CoM behavior given a foot contact point, a desired CoM kinematic path, and boundary conditions.

$$\begin{aligned} a_{\text{com}[z]} = &-\big(r^2 - p^2_{\text{com}[x]}\big)^{-1.5}\, p^2_{\text{com}[x]}\, v^2_{\text{com}[x]} \\ &-\big(r^2 - p^2_{\text{com}[x]}\big)^{-0.5}\, v^2_{\text{com}[x]} \\ &-\big(r^2 - p^2_{\text{com}[x]}\big)^{-0.5}\, p_{\text{com}[x]}\, a_{\text{com}[x]} \end{aligned} \tag{14}$$

where, r is the radius of the arc. Plugging the above acceleration in Equation (9) we get

$$a_{\text{com}[x]} = \Big(p_{\text{com}[x]} - p_{\text{cop}[kx]}\Big)\cdot \frac{N\Big(p_{\text{com}[x]}, v_{\text{com}[x]}, p_{\text{cop}[kx]}\Big)}{D\Big(p_{\text{com}[x]}, p_{\text{cop}_k[x]}, p_{\text{cop}_k[z]}\Big)}, \tag{15}$$

with

$$N \triangleq g - \Big(r^2 - p^2_{\text{com}[x]}\Big)^{-1.5} p^2_{\text{com}[x]}\, v^2_{\text{com}[x]} - \Big(r^2 - p^2_{\text{com}[x]}\Big)^{-0.5} v^2_{\text{com}[x]} \tag{16}$$

$$D \triangleq \Big(r^2 - p^2_{\text{com}[x]}\Big)^{0.5} - p_{\text{cop}_k[z]} + \Big(p_{\text{com}[x]} - p_{\text{cop}_k[x]}\Big)\Big(r^2 - p^2_{\text{com}[x]}\Big)^{-0.5} p_{\text{com}[x]}. \tag{17}$$

The acceleration of Equation (15) is non-linear and therefore cannot be integrated anymore.

In general, if the CoM geometric path is generated by a non-linear base function, the acceleration profile will be non-linear with general expression

$$a_{\text{com}[x]} = \Big(p_{\text{com}[x]} - p_{\text{cop}[kx]}\Big)\cdot \Phi\Big(p_{\text{com}[x]}, v_{\text{com}[x]}, p_{\text{cop}_k[x]}, p_{\text{cop}_k[z]}\Big), \tag{18}$$

where, $\Phi(.)$ is a non-linear function, and as such does not always have a closed-form solution. In Figure 2 we depict some hypothetical paths and their solution based on Equation (18). These solutions can be derived using numerical integration as we will soon describe.

For instance, let us consider the gap leaping maneuver shown in Figure 4. Two piecewise center of mass geometric paths are shown in Figure 1 as candidates to ascend the step. The top geometric path corresponds to a piecewise approximation of the captured motion from the human performing the maneuver and the one on the bottom

has been manually designed based on observation. Notice that both paths cover the complete gap leaping sequence which consists on jumping, flying, and landing phases. As such, the leaping maneuver involves two multi-contact and one single contact transitions. These transitions are not known a priori as it is the objective of the motion planner of Section IV-B to reveal them. Although both paths fulfill human and robot kinematic constraints, considering similar body segment dimensions, one of them is deficient as we will now reveal.

Because the geometric paths are piecewise linear, we consider Equation (13) for the single contact flight phase. Notice that, for our example, the numerator is positive since the center of mass is ahead of the left support foot. Therefore, if the denominator is positive the Sagittal CoM acceleration is positive and vice-versa, i.e.

$$\text{if} \quad a_i\, p_{\text{cop}[x]} + b_i > p_{\text{cop}_k[z]}, \quad \text{then} \quad a_{\text{com}[x]} > 0$$

$$\text{elseif} \quad a_i\, p_{\text{cop}[x]} + b_i < p_{\text{cop}_k[z]}, \quad \text{then} \quad a_{\text{com}[x]} < 0 \tag{19}$$

$$\text{else} \quad a_{\text{com}[x]} \to \infty. \tag{20}$$

Using the equality $b_i = p_{\text{com}[z]} - a_i\, p_{\text{com}[x]}$, derived from Equation (10), we can rewrite the above condition as

$$\text{if} \quad a_i < \frac{p_{\text{com}[z]} - p_{\text{cop}_k[z]}}{p_{\text{com}[x]} - p_{\text{cop}_k[x]}}, \quad \text{then} \quad a_{\text{com}[x]} > 0$$

$$\text{elseif} \quad a_i > \frac{p_{\text{com}[z]} - p_{\text{cop}_k[z]}}{p_{\text{com}[x]} - p_{\text{cop}_k[x]}}, \quad \text{then} \quad a_{\text{com}[x]} < 0 \tag{21}$$

$$\text{else} \quad a_{\text{com}[x]} \to \infty. \tag{22}$$

In other words, if the slope a_i is smaller than the slope of the line connecting the CoM to the supporting foot, then $a_{\text{com}[x]}$ is positive. On the other hand if a_i is larger than the slope of the CoM-foot line then $a_{\text{com}[x]}$ is negative. We call these conditions, the angle of attack of the CoM path. It can be calculated as the difference between the angles of the CoM path line and the CoM-foot line, i.e.

$$\alpha_{\text{attack}} = \text{atan}(a_i) - \text{atan}\left(\frac{p_{\text{com}[z]} - p_{\text{cop}_k[z]}}{p_{\text{com}[x]} - p_{\text{cop}_k[x]}}\right). \tag{23}$$

An interesting case, comes when the angle of attack is zero, i.e. when the slope of the CoM path a_i matches the slope of the CoM-foot line. In such case $a_{\text{com}[x]} \to \infty$. This condition is precisely the one that makes us rapidly jump. We can test it on ourselves by standing on one foot, starting moving forward, and then accelerating the CoM along the line connecting the foot on the ground. We will then see that we rapidly jump. In Figure 1 we show the angles of attack of the different CoM segments around the estimated flight phase. When the slope of the path segments is smaller than the line connecting the foot and the segment itself, then accelerations are positive, shown in green. Otherwise, the accelerations are negative, shown in red.

Using the angle of attack for analysis, we conclude that the top graph is feasible since there is a deceleration stage before reaching the vertical apex. This is consistent with the physics of free falling. However, the bottom graph is not feasible since there is an acceleration stage right before reaching the vertical apex which would cause the center of mass to overshoot the desired apex height instead of falling down on the path. The reason why there can exist a deceleration stage while moving forward as shown in the top graph, is because the inertial forces can be kept below the static friction cone if they have smaller a vertical component than the gravitational force.

D. Numerical integration

Our objective is to extract state-space trajectories for arbitrary kinematic CoM paths. We refer to perturbation theory to address the difficulty of solving non closed-form integrable differential equations such as Eq. (18). In particular, perturbation theory has been widely used to solve the trajectory of celestial bodies and pendulums. Perturbation theory, is a set of methods that enable to approximate solutions from problems that do not have exact solutions, by looking into the solution of an exact related problem. In our case, we have the exact solution of accelerations given positions and contact points and we seek to approximate the solution of the position versus the velocity, i.e. the state-space trajectory.

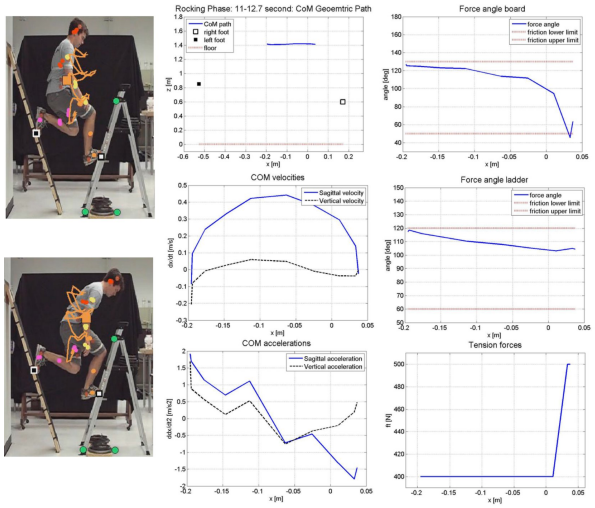

Fig. 3. **Analysis and estimation of internal tensions during a swinging maneuver:** In this figure we depict motion paths and state space curves of captured motion of a multi-contact swinging behavior as well as estimation of internal tensions using the multicontant/grasp matrix.

Let us study our generic Equation (18). For simplicity, we call $x \triangleq p_{\text{com}[x]}$ and therefore we can rewrite this Equation as

$$\ddot{x} = f(x, \dot{x}), \tag{24}$$

where $f(x, \dot{x})$ is the RHS of Equation (18). We assume that $\ddot{x}$ is approximately constant for small perturbations of x. We derive the first terms of a Taylor series for a small disturbance, ϵ, and for boundary conditions $(x_k, \dot{x}_k)$ we approximate the behavior of neighboring points as

$$\dot{x}_{k+1} \approx \dot{x}_k + \ddot{x}_k \epsilon, \tag{25}$$

$$x_{k+1} \approx x_k + \dot{x}_k \epsilon + 0.5\, \ddot{x}_k \epsilon^2. \tag{26}$$

From Eq. (25) we find an expression of the perturbation in terms of the velocities and acceleration, $\epsilon \approx (\dot{x}_{k+1} - \dot{x}_k)/\ddot{x}_k$, and substituting in Eq. (26), with $\ddot{x}_k = f(x_k, \dot{x}_k)$, we get

$$x_{k+1} \approx \frac{(\dot{x}_{k+1}^2 - \dot{x}_k^2)}{2\, f(x_k, \dot{x}_k)} + x_k, \tag{27}$$

which is the state-space approximate solution that we were looking for. The pipeline for finding state-space trajectories goes as follows: (1) choose a very small time perturbations ϵ, (2) given known velocities $\dot{x}_k$ and accelerations $\ddot{x}_k$, and using Eq. (25), we get the next velocity $\dot{x}_{k+1}$, (3) using Eq. (27) we get the next position x_{k+1}, (4) plot the points $(x_{k+1},\, \dot{x}_{k+1})$ in the phase-plane. We also notice, that we can iterate this recursion both forward and backward. If we iterate backward we then need to choose a negative perturbation ϵ. In Figure 2 we solve state space curves using perturbation theory for arbitrary linear and nonlinear paths and given various boundary conditions.

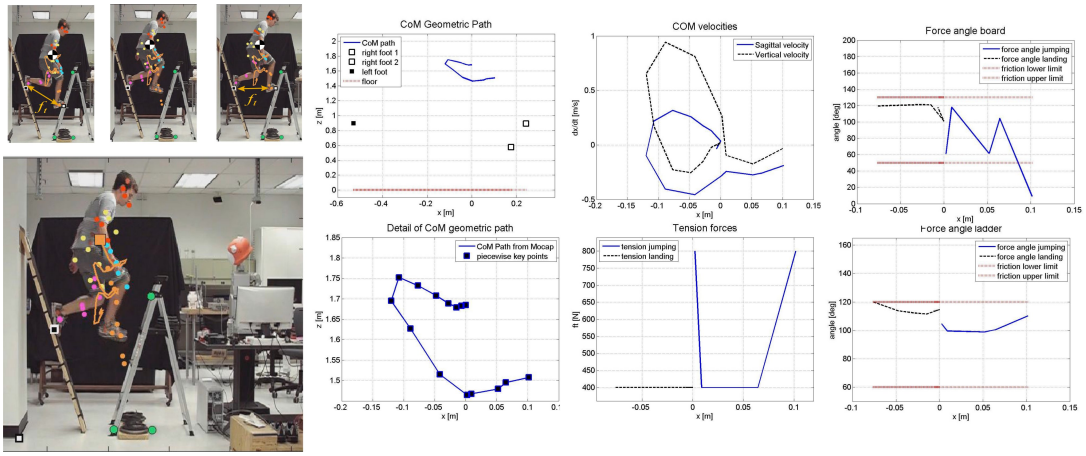

Fig. 4. **Analysis and estimation of internal tensions during jumping and landing maneuvers:** In this figure we depict a gap leaping maneuver and the extraction of data using motion capture devices.

IV. Case Studies

A. Analysis of extreme swinging behavior

Let us consider the multi-contact swinging behavior shown in Figure 3, where the subject swings his body back and forth between two points. Suppose that we have a known center of mass phase diagram of the maneuver, for instance extracted through mocap (see graphs included in the Figure). There are infinite solutions to move along the same kinematic path. However, each of them carries a different signature in terms of velocities and internal tensions. We use Equation (5) to extract internal tension forces by searching solutions that fulfill the friction properties of the surfaces in contact (see Algorithm 1 for details). As such, during multi-contact, the problem that we solve is determining whether the phase curves are feasible given the friction properties of the surfaces in contact.

On the image sequence, student Nick Paine engages into a forceful contact behavior between the wall board and the ladder to enable fast swings back and forth. The wall board leans at an angle of 70^o from the floor and contains layers of adhesive sand paper to increase the friction coefficient with respect to the sport shoes. A simple mocap setup is used in the HCRL facilities at UT Austin, where multiple markers are placed near Nick's center of mass body segments, while a video camera records the movement from a sufficient distance and at a rate of 30 frames per second. The video sequence is then broken into multiple jpeg images and then uploaded into Matlab using the command `imread()`. In Matlab, we use the command `ginput()` to track the 14 markers as well as the perceived feet center of pressure points. We use male anthropometry data ratios from [28], adjusted to Nick's weight and composition, to extract the center of mass path. The continuous yellow curve corresponds to the center of mass path from the bottom of the ladder until reaching the step where the swings occur.

After extracting the path, we use the Matlab tool `cftool()` to fit a spline using piecewise polynomials and then we extract the first and second derivatives to estimate velocities and accelerations of the center of mass. The graphs on the center column of Figure 3 display, (1) the path of the center of mass, (2) state space curves of the Sagittal and vertical center of mass behavior, and (3) estimated accelerations. The graphs on the rightmost column show the result of extracting estimated internal tension forces f_t that fulfill the friction characteristics of the surfaces and the resulting reaction forces. They plot the right foot reaction force angle against the ladder's friction angle and the left foot reaction force angle against the board's friction angle. They also plot the estimated internal tension force derived from the search strategy of Algorithm 1, which is found to oscillate between 400-500[N].

B. Synthesis of gap leaping maneuver

We now consider the maneuver of leaping from a given ladder step to a higher one as shown in Figure 4. To tackle this problem we resort to the two powerful methods presented in Sections III-A and III-D, namely the multi-contact/grasp matrix and the perturbation recursions. In the sequence shown in Figure 4, student Nick Paine leaps upward from the second to the third step of the ladder and by means of the supporting wall board.

Algorithm 1 Motion planner for multi-contact jumping (forward) and landing (backward) phases

choose perturbation $\epsilon > 0$ for forward or $\epsilon < 0$ for backward rec.
use Eq. (2) to compute multi-contact/grasp matrices $C_{k(\forall k)}$
use Eq. (4) to compute $C_{fk(\forall k)}$, $C_{tk(\forall k)}$
using Eq. (5) to search over feasible $\ddot{x}_{k(\forall k)}$ and $f_{tk(\forall k)}$ values
set $x_{k(k=1)}$ equal to start (forward) or end (backward) point
set $\dot{x}_{k(k=1)} = 0$ and $\dot{z}_{k(k=1)} = 0$ due to boundary conditions
while distance to forward / backward horizon $\neq 0$ **do**
  extract $z_{k+1} = a_i\ x_k + b_i$
  extract $\ddot{z}_{k+1} = \ddot{x}_{k+1}/a_i$
  use Eq. (26) to infer $\dot{z}_{k+1}$
  use Eq. (27) to infer z_{k+1}
  extract $x_{k+1} = (z_{k+1} - b_i)/a_i$
  extract $\dot{x}_{k+1} = \dot{z}_{k+1}/a_i$
  change piecewise segments $(a_i,\ b_i)$ when appropriate
  use Eq. (5) to determine reaction forces f_{rk}
  check that reaction forces f_{rk} are within friction cones
end while

Our approach can be summarized as follows. First we derive a center of mass geometric path using the techniques presented in Section III-C. We then consider three distinctive phases corresponding to a multi-contact jumping phase, a single-contact flight phase, and a multi-contact landing phase. Based on the designed path, we first solve the single-contact flight phase by means of perturbation theory recursion. Next, we solve the jumping and landing phases by means of the the multi-contact/grasp matrix and also the perturbation theory recursion. Finally, we implement a contact transition planner, based on finding intersection points in state space between multi-contact and single-contact phases.

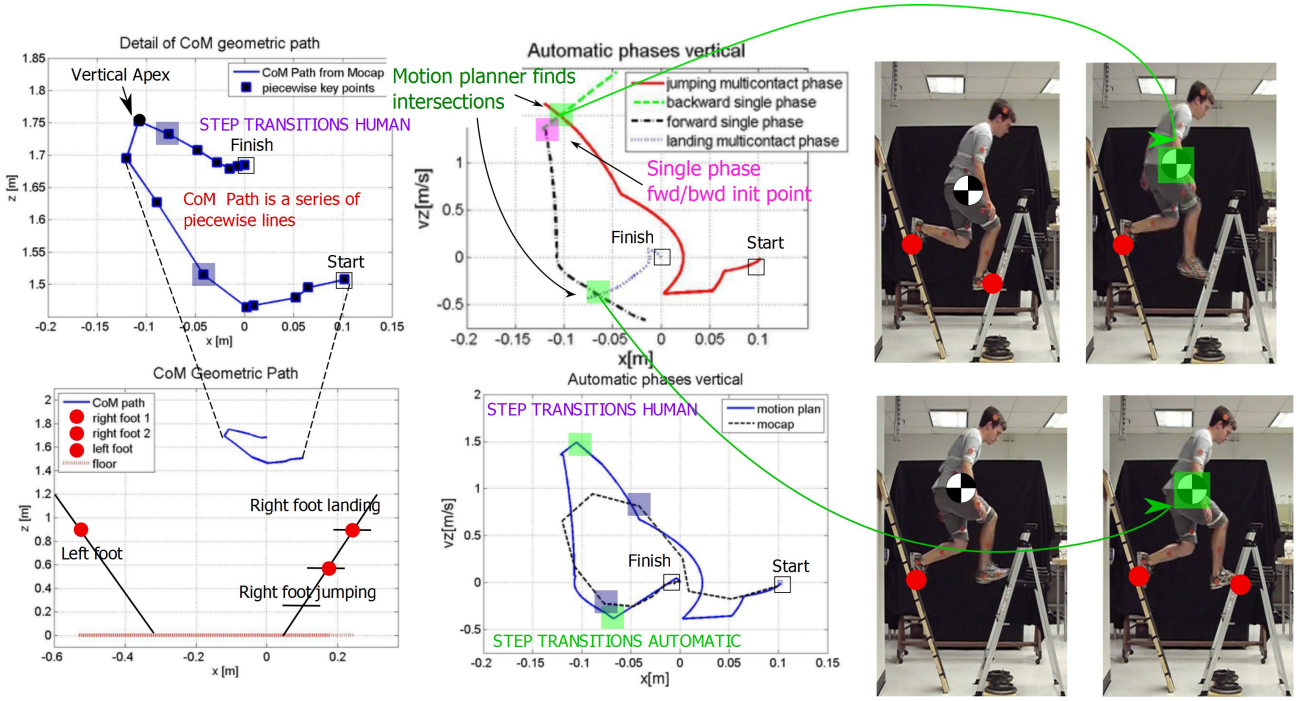

Fig. 5. **Contact transition planner for gap leaping:** This composed figure depicts details on the planning strategy to synthesize the leaping maneuver.

Before starting with the synthesis part, let us analyze the behavior shown in Figure 4. Nick accelerates his body backward (jumping phase) to gain momentum to leap upward (flight phase) and land on the next ladder step (landing phase). Motion capture is conducted enabling the extraction of CoM geometric paths and CoM state space curves as shown in the graphs that accompany the Figure. We then approximate the CoM path using piecewise segments. Since we lack force plates on the surfaces in contact, we estimate contact reaction forces by using Algorithm 1. The results of this estimation is shown in the center bottom graph.

We now consider synthesizing an artificially generated maneuver that can leap the steps in similar ways than the human does. The results of this process are shown in Figure 6. For simplicity, we use the discretized version of the CoM geometric path from the human shown on the bottom left graph of Figure 4. We divide the synthesis problem in three separate parts. First, we use Algorithm 2 to derive flight phase data. This algorithm can be summarize as follows. We choose an initial point on the CoM geometric path perceived as belonging to the single-contact flight phase. We then search over candidate starting vertical velocities and apply perturbation theory to derive the natural dynamics of the movement over the geometric path. We validate the initial velocity if its forward projection reaches the vertical apex with zero vertical velocities, meaning that the center of mass can start falling. Because we don't know to what extend the single-contact phase belongs to the different segments of the CoM geometric path we implement forward and backward recursions over horizons along the path.

We then solve the multi-contact jumping and landing phases by means of Algorithm 1 which can be summarized as follows. We compute the multi-contact grasp matrix along all data points over the CoM geometric path. We then search over candidate acceleration and tension pairs and apply perturbation theory to project the movement over a horizon. The jumping phase involves a forward projection while the landing phase involves a backward projection which need to be considered in choosing the perturbation sign direction. Putting together the previous single and multi-contact recursions lead to the

Algorithm 2 Motion planner for single-contact flight phase (forward/backward strategy)

{forward recursion}
choose perturbation $\epsilon > 0$
set $x_{k(k=1)}$ to be on flight zone
search $\dot{z}_{k(k=1)}$ to reach vertical apex
while distance to forward horizon $\neq 0$ **do**
  extract $z_k = a_i\ x_k + b_i$
  use Eq. (13) to determine $\ddot{x}_k$
  extract $\ddot{z}_k = a_i\ \ddot{x}_k$
  use Eq. (26) to infer $\dot{z}_{k+1}$
  use Eq. (27) to infer z_{k+1}
  extract $x_{k+1} = (z_{k+1} - b_i)/a_i$
  extract $\dot{x}_{k+1} = \dot{z}_{k+1}/a_i$
  change piecewise segments $(a_i,\ b_i)$ when appropriate
  check that $\dot{z}_{k(k=apex)} = 0$
end while
{backward recursion}
choose perturbation $\epsilon < 0$
use $x_{k(k=1)}$ equal to previous init value
use $\dot{z}_{k(k=1)}$ from previous vertical apex search
while distance to backward horizon $\neq 0$ **do**
  extract $z_k = a_i\ x_k + b_i$
  use Eq. (13) to determine $\ddot{x}_k$
  extract $\ddot{z}_k = a_i\ \ddot{x}_k$
  use Eq. (26) to infer $\dot{z}_{k+1}$
  use Eq. (27) to infer z_{k+1}
  extract $x_{k+1} = (z_{k+1} - b_i)/a_i$
  extract $\dot{x}_{k+1} = \dot{z}_{k+1}/a_i$
  change piecewise segments $(a_i,\ b_i)$ when appropriate
end while

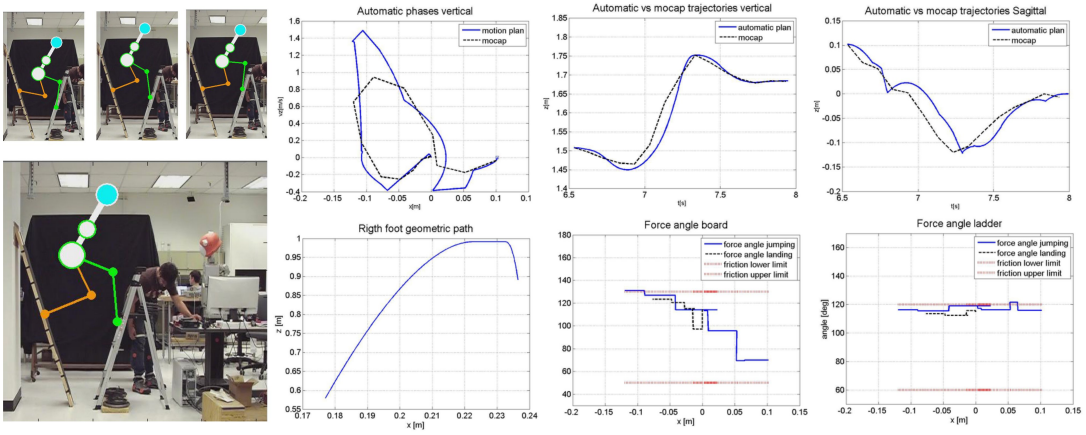

Fig. 6. **Results on synthesis of gap leaping using motion planner:** Synthetic leaping motion and artificially generated path and contact plans to achieve it.

top center graph of Figure 5. As we can see, the jumping and landing phases intersect the flight phase at different points (shown in green on the graph).

Having solved all phases of the movement, we consider finding contact transitions by means of a contact planner. Because we operate in state space, crossing points between phases imply continuity on position and velocity. As such, the intersections previously discussed are precisely the moments at which contacts need to change to follow the path. For instance, to switch from jumping to free flight phase, we need to remove the right foot contact at the intersection between the jumping and the backward flight phases. The final motion plan is shown on the bottom center graph of Figure 5 against the one extracted from the human. As we can notice they are remarkably similar. One of the main differences is that the synthetic path reaches higher velocities during the jumping phase than what the mocap data extraction process shows. However, when synthesizing the movement based on the proposed planner, shown in Figure 6, the time trajectories of the vertical and Sagittal CoM behavior look very similar to the human. Therefore, we believe that the difference in velocities are due to the low sampling rate of the marker data. In fact, the sampling time is equal to $0.1[s]$ which means that the peak velocities may have been cut off.

Figure 6 depicts the synthetic maneuver based on the planning strategy we have proposed. A time based reconstruction of the vertical and Sagittal trajectories is also shown against the same data extracted from the human. The trajectories are very similar, demonstrating the validity of the proposed planning methodology. Also, reaction forces of the synthetic maneuver are shown to remain within boundaries of the surfaces in contact. Finally, we show the right foot geometric path created with a trajectory generator (not described here) to ascend one step.

V. Conclusion

Maneuvering in extreme environments is a highly complex problem because of the lack of closed-form solutions of the passive dynamics and the dominance of multi-contact forces during take off and landing phases. It requires an in-depth exploration of physical phenomena and resorting to advanced mathematical tools to model and solve these type of interactions. We have resorted to multi-contact dynamics and numerical integration to derive state space curves during the different phases of the movements. These tools, and proposing a contact solver based on finding intersection points in state space represent important contributions for legged robots.

The good correlation of synthetic curves shown in Figure 6, which compare artificial and human movement, point towards the validity of our methods. However, there is still much work to be done. Topics to explore in the near future include, (1) the inclusion of center of mass inertial moments in the modeling and planning strategies, (2) relying less on manual search of data points, and (3) extending the methods to 3d maneuvers. Moreover, to be deployable, our methods will need to be extended with a suitable control strategy as well as the design of bipedal hardware that can accomplish the performance sought.

Appendix

A. Simple virtual linkage model for the human

Using dynamic balance of moments and forces we can specify the following relationship which links inertial and gravitational behavior to reaction forces (see [27] for the derivation of this model)

$$\begin{pmatrix} [I]_{3\times3} & [I]_{3\times3} \\ \hat{P}_{\mathrm{cop}[1]} & \hat{P}_{\mathrm{cop}[2]} \end{pmatrix} \begin{pmatrix} f_{r1} \\ f_{r2} \end{pmatrix} = \begin{pmatrix} [I]3\times3 & [0]_{3\times3} \\ \hat{P}_{\mathrm{com}} & [I]_{3\times3} \end{pmatrix} \begin{pmatrix} f_{\mathrm{com}} + Mg \\ m_{\mathrm{com}} \end{pmatrix}, \quad (28)$$

where the operators with a $\hat{(\cdot)}$ correspond to the cross product matrix, $p_{\mathrm{cop}[i]}$ corresponds to the center of pressure of the i-th foot and p_{com} corresponds to the position of the center of mass. We can also express internal forces as

$$f_t = S_t \left({}^{VL}R_0\right) \Delta_t \begin{pmatrix} f_{r1} \\ f_{r2} \end{pmatrix}, \quad (29)$$

where the differential operation is described by

$$\Delta_t \triangleq \begin{pmatrix} [I]3\times3 & [I]_{3\times3} \end{pmatrix}, \quad (30)$$

and the rotation matrix that transforms an inertial frame to the virtual linkage frame is

$${}^{0}R_{VL} \triangleq \begin{pmatrix} (x_{VL}\cdot\hat{x}) & (x_{VL}\cdot\hat{y}) & (x_{VL}\cdot\hat{z}) \\ (y_{VL}\cdot\hat{x}) & (y_{VL}\cdot\hat{y}) & (y_{VL}\cdot\hat{z}) \\ (z_{VL}\cdot\hat{x}) & (z_{VL}\cdot\hat{y}) & (z_{VL}\cdot\hat{z}) \end{pmatrix}, \quad (31)$$

Calling

$$\left[W_{\mathrm{com}}\right]_{6\times6} \triangleq \begin{pmatrix} [I]3\times3 & [0]_{3\times3} \\ \hat{P}_{\mathrm{com}} & [I]_{3\times3} \end{pmatrix}^{-1} \begin{pmatrix} [I]_{3\times3} & [I]_{3\times3} \\ \hat{P}_{\mathrm{cop}[1]} & \hat{P}_{\mathrm{cop}[2]} \end{pmatrix} \quad (32)$$

$$\left[W_{\mathrm{int}}\right]_{1\times6} \triangleq S_t \left({}^{VL}R_0\right) \Delta_t, \quad (33)$$

we get a non-square multi-contact expression

$$\begin{pmatrix} f_{\text{com}} + M\,g \\ m_{\text{com}} \\ f_t \end{pmatrix} = [C]_{7\times 6} \begin{pmatrix} f_{r1} \\ f_{r2} \end{pmatrix}, \tag{34}$$

with

$$[C]_{7\times 6} \triangleq \left(\begin{array}{c} \left[W_{\text{com}}\right]_{6\times 6} \\ \hline \left[W_{\text{int}}\right]_{1\times 6} \end{array}\right) \tag{35}$$

The matrix $[C]_{7\times 6}$ is a candidate for the multi-contact/grasp matrix, however being non-square it means that there is redundancy on the RHS of the above equation. We need to reveal the interdependency between inertial and reaction forces. This is analogous to the case analyzed in our previous paper [27] where in planar dual contact stance we revealed that there is a dependency between the zero moment position and the position of the contact centers of pressure. A similar condition must exist in the case of non-coplanar dual contact stance. For instance, imagine the static case where the center of mass lies in the line uniting the two point feet. Then it seems physically intuitive that no accelerations can be caused in the directions lateral to the uniting line (i.e. the y direction on the virtual linkage frame). We decide to remove the inertial forces on the y direction. For that, we choose a selection matrix of the following form

$$S_{\text{VL}} \triangleq \left(\begin{array}{c|c|c} \begin{matrix} 1 & 0 & 0 \\ 0 & 0 & 1 \end{matrix} & [0]_{2\times 3} & [0]_{1\times 3} \\ \hline [0]_{3\times 3} & [I]_{3\times 3} & [0]_{3\times 1} \\ \hline [0]_{1\times 3} & [0]_{1\times 3} & 1 \end{array}\right) \epsilon\, \mathcal{R}^{6\times 7} \tag{36}$$

Taking independent variables we formulate the multi-contact/grasp matrix

$$[C]_{6\times 6} \triangleq S_{\text{VL}} \left(\begin{array}{c} \left[W_{\text{com}}\right]_{6\times 6} \\ \hline \left[W_{\text{int}}\right]_{1\times 6} \end{array}\right). \tag{37}$$

Acknowledgements

Many thanks to HCRL students Nick Paine and Somudro Gupta for their assistance on the experiments and for providing feedback on the theoretical content.

References

[1] K. Harada, S. Kajita, K. Kaneko, and H. Hirukawa, "Zmp analysis for arm/leg coordination," in *Proceedings of the IEEE/RSJ International Conference on Intelligent Robots and Systems*, Las Vegas, USA, October 2003, pp. 75–81.

[2] S. Kajita, M. Morisawa, K. Harada, K. Kaneko, F. Kanehiro, K. Fujiwara, and H. Hirukawa, "Biped walking pattern generator allowing auxiliary zmp control," in *Intelligent Robots and Systems, 2006 IEEE/RSJ International Conference on*, october 2006, pp. 2993–2999.

[3] M. Raibert, *Legged Robots that Balance*. MIT Press, Cambridge, Ma., 1986.

[4] T. Bretl and S. Lall, "Testing static equilibrium for legged robots," *IEEE Transactions on Robotics*, vol. 24, no. 4, pp. 794–807, August 2008.

[5] C. Collette, A. Micaelli, C. Andriot, and P. Lemerle, "Robust balance optimization control of humanoid robots with multiple non coplanar grasps and frictional contacts," in *Proceedings of the IEEE International Conference on Robotics and Automation*, Pasadena, USA, May 2008.

[6] J. Pratt and R. Tedrake, "Velocity-based stability margins for fast bipedal walking," in *Fast Motions in Biomechanics and Robotics*, M. Diehl and K. Mombaur, Eds., 2006, vol. 340, pp. 299–324.

[7] T. McGeer, "Passive dynamic walking," *The International Journal of Robotics Research*, vol. 9, no. 2, pp. 62–68, 1990.

[8] A. Goswami, B. Espiau, and A. Kermane, "Limit cycles and their stability in a passive bipedal gait," in *Proceedings of the IEEE International Conference on Robotics and Automation*, April 1996, pp. 246–251.

[9] K. Mombaur, H. Bock, J. Schloder, and R. Longman, "Self-stabilizing somersaults," *Robotics, IEEE Transactions on*, vol. 21, no. 6, pp. 1148 – 1157, december 2005.

[10] M. Coleman and A. Ruina, "An uncontrolled toy that can walk but cannot stand still," *Physical Review Letters*, vol. 80, no. 16, pp. 3658–3661, 1998.

[11] S. Collins, A. Ruina, R. Tedrake, and M. Wisse, "Efficient bipedal robots based on passive-dynamic walkers," *Science Magazine*, vol. 307, no. 5712, pp. 1082–1085, 2005.

[12] A. Ruina, J. Bertram, and M. Srinivasan, "A collisional model of the energetic cost of support work qualitatively explains leg sequencing in walking and galloping, pseudo-elastic leg behavior in running and the walk-to-run transition," *Journal of Theoretical Biology*, no. 237, pp. 170–192, 2005.

[13] T. Takuma and K. Hosoda, "Controlling the walking period of a pneumatic muscle walker," *The International Journal of Robotics Research*, vol. 25, no. 9, pp. 861–866, 2006.

[14] E. Westervelt, J. Grizzle, C. Chevallereau, J. Choi, and B. Morris, *Feebdack control of dynamic bipedal robt locomotion*. CRC Oress, 2007.

[15] B. Stephens and C. Atkeson, "Modeling and control of periodic humanoid balance using the linear biped model," in *Humanoid Robots, 2009. Humanoids 2009. 9th IEEE-RAS International Conference on*, december 2009, pp. 379 –384.

[16] J. Rummel, Y. Blum, and A. Seyfarth, "Robust and efficient walking with spring-like legs," *Bioinspiration & Biomimetics*, vol. 5, no. 4, p. 046004, 2010.

[17] M. Wisse, A. Schwab, R. van der Linde, and F. van der Helm, "How to keep from falling forward: elementary swing leg action for passive dynamic walkers," *Robotics, IEEE Transactions on*, vol. 21, no. 3, pp. 393 – 401, june 2005.

[18] K. Byl and R. Tedrake, "Metastable walking machines," *The International Journal of Robotics Research*, vol. 28, no. 8, pp. 1040–1064, 2009.

[19] R. Tedrake, "Applied optimal control for dynamically stable legged locomotion," Ph.D. dissertation, MIT, Cambridge, USA, 2004.

[20] I. R. Manchester, U. Mettin, F. Iida, and R. Tedrake, "Stable dynamic walking over uneven terrain," *The International Journal of Robotics Research*, vol. 30, no. 3, pp. 265–279, 2011.

[21] M. Spong, J. Holm, and D. Lee, "Passivity-based control of bipedal locomotion," *Robotics Automation Magazine, IEEE*, vol. 14, no. 2, pp. 30 –40, june 2007.

[22] M. Zucker, J. Bagnell, C. Atkeson, and J. Kuffner, "An optimization approach to rough terrain locomotion," in *Robotics and Automation (ICRA), 2010 IEEE International Conference on*, may 2010, pp. 3589 –3595.

[23] K. Hauser, T. Bretl, K. Harada, and J. Latombe, "Using motion primitives in probabilistic sample-based planning for humanoid robots," in *Workshop on Algorithmic Foundations of Robotic (WAFR)*, New York, USA, July 2006.

[24] K. Bouyarmane and A. Kheddar, "Multi-contact stances planning for multiple agents," in *Proceedings of the IEEE International Conference on Robotics and Automation*, Shanghai, May 2011.

[25] L. Sentis and B. Fernandez, "Com state space cascading manifolds for planning dynamic locomotion in very rough terrain," in *Proceedings of Dynamic Walking 2011*, Jena, Germany, July 2011.

[26] ——, "Perturbation theory to plan dynamic locomotion in very rough terrains," in *IEEE/RSJ International Conference on Intelligent Robots and Systems*, September 2011.

[27] L. Sentis, J. Park, and O. Khatib, "Compliant control of multi-contact and center of mass behaviors in humanoid robots," *IEEE Transactions on Robotics*, vol. 26, no. 3, pp. 483–501, June 2010.

[28] H. Armstrong, *Anthropometry and mass distribution for human analogues*. Military male aviators, 1988.